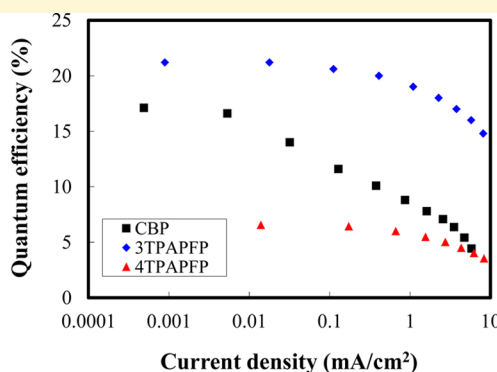
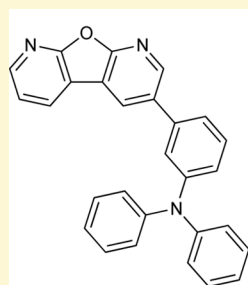


Above 20% External Quantum Efficiency in Thermally Activated Delayed Fluorescence Device Using Furodipyridine-Type Host Materials

Yirang Im and Jun Yeob Lee*

Department of Polymer Science and Engineering, Dankook University 126, Jukjeon-dong, Suji-gu, Yongin, Gyeonggi 448-701, Korea

Supporting Information



ABSTRACT: High efficiency green thermally activated delayed fluorescence device with a quantum efficiency above 20% was developed using a bipolar host material, 3-(furo[2,3-b:5,4-b']dipyridin-3-yl)-*N,N*-diphenylaniline (3TPAPFP), derived from furodipyridine core structure. The furodipyridine based 3TPAPFP showed a singlet and triplet energy for efficient energy transfer to thermally activated delayed fluorescent dopant, (4*s*,6*s*)-2,4,5,6-tetra(9*H*-carbazol-9-yl)isophthalonitrile (4CzIPN), and bipolar charge transport properties for balanced hole and electron density. A high quantum efficiency of 21.2% was achieved in the fluorescent device using the 3TPAPFP host doped with 4CzIPN dopant at a very low doping concentration of 1%.

INTRODUCTION

External quantum efficiency (EQE) is one of important device performances of organic light-emitting diodes (OLEDs), and there have been a lot of studies to improve the EQE of OLEDs. In most cases, phosphorescent OLEDs has been studied to enhance the EQE of OLEDs because of the 4-fold higher EQE of phosphorescent OLEDs than that of fluorescent OLEDs.¹ Theoretically, phosphorescent OLEDs can utilize both singlet and triplet excitons for light emission, whereas fluorescent OLEDs can use only singlet excitons for light emission. Therefore, it was very difficult to achieve high EQE above 10% in fluorescent OLEDs.^{2–4} However, thermally activated delayed fluorescence (TADF) has been reported recently, and high EQE of 19.3% was reported in green fluorescent OLEDs.⁵

Two types of delayed fluorescence, triplet fusion and TADF, have been reported to enhance the EQE of fluorescent OLEDs. Both processes use up-conversion of triplet excited state to singlet excited state for extra light emission in addition to singlet emission of common fluorescent OLEDs. Theoretical maximum internal quantum efficiency of triplet fusion device is 62.5% because two triplet excitons can be converted into one singlet exciton,^{6,7} whereas that of the TADF device is 100% because all triplet excitons can be converted into singlet exciton.⁵ Therefore, the TADF OLEDs can be comparable to phosphorescent OLEDs in terms of EQE and are promising as

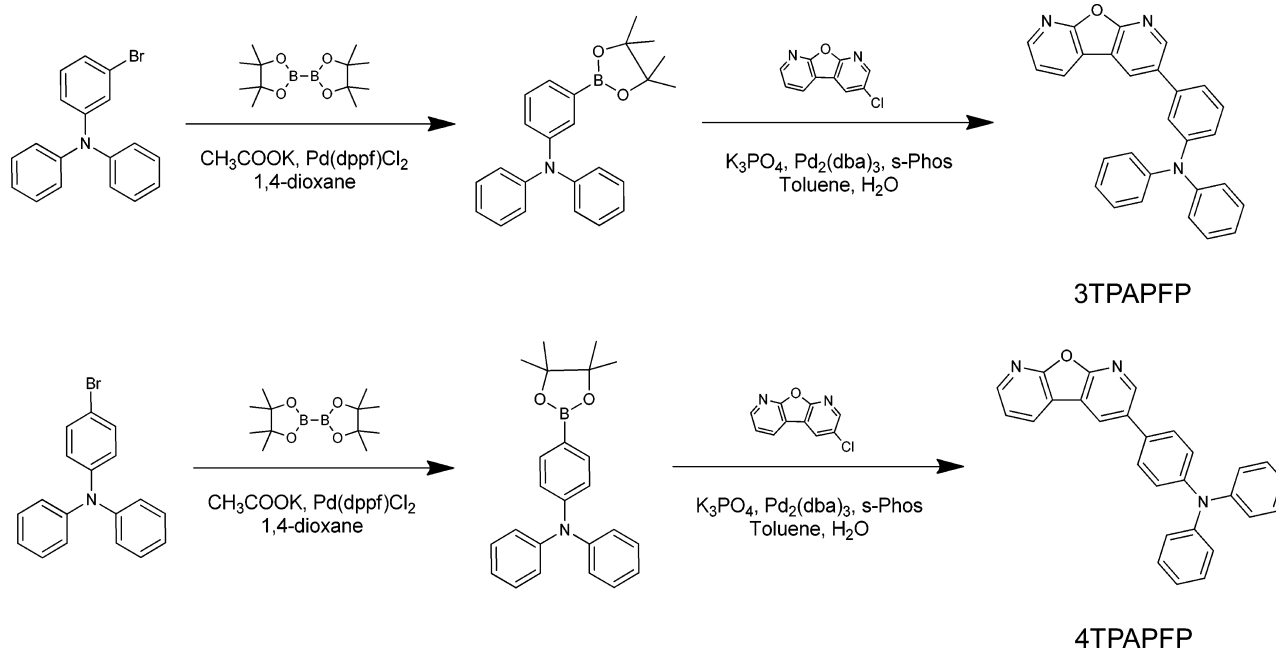
the fluorescent OLED device, which can compete with phosphorescent OLEDs even though the current EQE of the TADF OLEDs is still not comparable to that of phosphorescent OLEDs.

Several TADF materials have been developed,^{5,8–17} and (4*s*,6*s*)-2,4,5,6-tetra(9*H*-carbazol-9-yl)isophthalonitrile (4CzIPN) was effective as a green TADF emitter.⁵ The 4CzIPN emitter showed very small singlet and triplet energy difference and efficient up-conversion of triplet excitons into singlet excitons. The 4CzIPN emitter was doped into a 4,4'-di(9*H*-carbazol-9-yl)biphenyl (CBP) host material, and a high quantum efficiency of 19.3% was achieved in green TADF device by optimizing the device structure. However, the CBP host is not an ideal host material for the 4CzIPN device because of the rather strong hole transport properties and incomplete energy transfer at low doping concentration. Therefore, it is strongly required to develop new host materials that can improve the EQE of 4CzIPN device. Ideal host materials for the TADF dopant much have high singlet and triplet energy for energy transfer, the highest occupied molecular orbital (HOMO) and the lowest unoccupied

Received: October 19, 2013

Revised: January 10, 2014

Scheme 1. Synthetic Scheme of 3TPAPFP and 4TPAPFP



molecular orbital (LUMO) for exciton blocking, large overlap of the host PL emission with dopant absorption and bipolar charge transport properties for charge balance.

In this work, two host materials, 3-(furo[2,3-b:5,4-b']dipyridin-3-yl)-*N,N*-diphenylaniline (3TPAPFP) and 4-(furo[2,3-b:5,4-b']dipyridin-3-yl)-*N,N*-diphenylaniline (4TPAPFP), were developed as bipolar host materials for the 4CzIPN TADF emitter. The 4CzIPN emitter was doped into the host materials, and a high EQE of 21.2% at very low doping concentration of 1% was demonstrated using 3TPAPFP:4CzIPN emitting layer. This is the first work reporting above 20% EQE in fluorescent OLED device.

EXPERIMENTAL SECTION

General Information. 3-Bromo-*N,N*-diphenylaniline, 4-bromo-*N,N*-diphenylaniline, bis(pinacolato)diboron, [1,1'-bis-(diphenylphosphino)ferrocene]dichloropalladium(II) (Pd(dppf)Cl₂), tris(dibenzylideneacetone)dipalladium(0) (Pd₂(dba)₃), and 2-dicyclohexylphosphino-2',6'-dimethoxybiphenyl (S-Phos) (P&H Tech Co.) were used without further purification. Potassium acetate (CH₃COOK), potassium phosphate (K₃PO₄) (Aldrich Chem. Co.), and 1,4-dioxane (Duksan Sci. Co.) were also used as received. Toluene was distilled over sodium and calcium hydride. 3-Chlorofuro[2,3-b:5,4-b']dipyridine was synthesized according to the method reported in the literature.¹⁸

The ¹H and ¹³C nuclear magnetic resonance (NMR) was recorded on an Avance 500 (500 MHz) spectrometer. Fluorescence spectrophotometer (HITACHI, F-7000) and ultraviolet–visible (UV–vis) spectrophotometer (Shimadzu, UV-2501PC) were used to measure photoluminescence (PL) spectra and UV–vis spectra. Low temperature PL measurement of the synthesized materials was carried out at 77 K using a dilute solution of the materials. The differential scanning calorimeter (DSC) measurements were performed using a Mettler DSC 822e under nitrogen at a heating rate of 10 °C/min to measure the melting point (*T*_m) and glass transition temperature (*T*_g). The mass spectra were recorded using a JEOL JMS-700 spectrometer in FAB mode and elemental analysis were recorded using a CE instrument Flash 2000. The HOMO energy levels were measured with a cyclic voltammetry (CV). CV measurement of organic materials was carried out in acetonitrile solution with tetrabutylammonium perchlorate at 0.1 M concentration. Ag was used as the reference

electrode and Pt was the counter electrode. Organic materials were coated on carbon electrodes and were immersed in electrolyte for analysis. Oxidation and reduction scans of the materials were separately carried out and reduction scans were carried out after nitrogen bubbling. The delayed PL spectra of the organic films was measured using a pulsed Nd–YAG laser (355 nm) as the excitation light source and a monochromator attached with a photomultiplier tube was used as the optical detector system.

Synthesis. Synthetic scheme of the 3TPAPFP and 4TPAPFP compounds are described in Scheme 1.

***N,N*-Diphenyl-3-(4,4,5,5-tetramethyl-1,3,2-dioxaborolan-2-yl)aniline (1).** 3-bromo-*N,N*-diphenylaniline (10 g, 30.84 mmol), bis(pinacolato)diboron (9.40 g, 37.01 mmol), CH₃COOK (9.08 g, 92.52 mmol), and Pd(dppf)Cl₂ (0.76 g, 0.93 mmol) were dissolved in 1,4-dioxane under nitrogen atmosphere. The reaction mixture was stirred and refluxed for 24 h. The mixture was filtered, diluted with ethyl acetate, and washed with distilled water. The organic layer was dried over anhydrous MgSO₄ and evaporated in vacuo to give the crude product. The extract was evaporated to dryness, affording a solid, which was further purified by column chromatography by ethyl acetate/*n*-hexane.

Yield 73%, ¹H NMR (500 MHz, CDCl₃): δ 7.59 (s, 1H, *J* = 2 Hz), 7.49 (d, 1H, *J* = 3.75 Hz), 7.26 (t, 1H, *J* = 5 Hz), 7.21 (t, 4H, *J* = 5.5 Hz), 7.17 (d, 1H, *J* = 5.75 Hz), 7.04 (d, 4H, *J* = 3.75 Hz), 6.96 (t, 2H, *J* = 4.83 Hz), 1.30 (s, 12H). MS (FAB) *m/z*: 371 [(*M* + *H*)⁺].

***N,N*-Diphenyl-4-(4,4,5,5-tetramethyl-1,3,2-dioxaborolan-2-yl)aniline (2).** 4-bromo-*N,N*-diphenylaniline (10 g, 30.84 mmol), bis(pinacolato)diboron (9.40 g, 37.01 mmol), CH₃COOK (9.08 g, 92.52 mmol), and Pd(dppf)Cl₂ (0.76 g, 0.93 mmol) were dissolved in 1,4-dioxane under nitrogen atmosphere. The reaction mixture was stirred and refluxed for 24 h. The mixture was filtered, diluted with ethyl acetate, and washed with distilled water. The organic layer was dried over anhydrous MgSO₄ and evaporated in vacuo to give the crude product. The extract was evaporated to dryness, affording a solid, which was further purified by column chromatography by ethyl acetate/*n*-hexane.

Yield 61%, ¹H NMR (500 MHz, CDCl₃): δ 7.66 (d, 2H, *J* = 4.25 Hz), 7.24 (t, 4H, *J* = 5.17 Hz), 7.10 (d, 4H, *J* = 4 Hz), 7.03 (t, 4H, *J* = 4.83 Hz), 1.33 (s, 12H). MS (FAB) *m/z*: 371 [(*M* + *H*)⁺].

3-(Furo[2,3-b:5,4-b']dipyridin-3-yl)-*N,N*-diphenylaniline (3TPAPFP). *N,N*-diphenyl-3-(4,4,5,5-tetramethyl-1,3,2-dioxaborolan-2-yl)aniline (1) (2.18 g, 5.87 mmol), 3-chlorofuro[2,3-b:5,4-b']dipyridine (3) (1 g, 4.89 mmol), K₃PO₄ (3.11 g, 14.67 mmol), and S-

Phos (0.3 g, 0.73 mmol) were dissolved in toluene and distilled water under bubbling with nitrogen for 30 min. Pd₂(dba)₃ (0.14 g, 0.15 mmol) was added to the solution, and the resulting solution was refluxed for 24 h under nitrogen atmosphere. The mixture was diluted with ethyl acetate and washed with distilled water. The organic layer was dried over anhydrous MgSO₄ and evaporated in vacuo to give the crude product. The extract was evaporated to dryness, affording a white solid, which was further purified by column chromatography by ethyl acetate/*n*-hexane.

Yield = 74%. *T_g* = 67 °C. *T_m* = 219 °C. ¹H NMR (500 MHz, CDCl₃): δ 8.61 (s, 1H, *J* = 2.5 Hz), 8.51 (d, 1H, *J* = 3.25 Hz), 8.33 (s, 1H, *J* = 2.5 Hz), 8.28 (d, 1H, *J* = 4.75 Hz), 7.37 (m, 3H), 7.27 (m, 5H), 7.16 (d, 4H, *J* = 3.75 Hz), 7.12 (d, 1H, *J* = 4.75 Hz), 7.05 (t, 2H, *J* = 4.83 Hz). ¹³C NMR (500 MHz, CDCl₃): δ 162.1, 161.1, 148.8, 147.7, 147.6, 146.5, 138.7, 133.6, 130.5, 130.0, 129.4, 128.7, 124.5, 123.2, 123.1, 122.3, 121.3, 119.8, 115.6, 115.4. MS (FAB) *m/z*: 414 [(M + H)⁺]. Anal. Calcd for C₂₈H₁₉N₃O: C, 81.34; H, 4.63; N, 10.16; O, 3.87. Found: C, 81.03; H, 4.64; N, 10.02; O, 3.94.

4-(Furo[2,3-*b*:5,4-*b'*]dipyridin-3-yl)-*N,N*-diphenylaniline (4TPAPFP). *N,N*-diphenyl-4-(4,4,5,5-tetramethyl-1,3,2-dioxaborolan-2-yl)aniline (2) (2.18 g, 5.87 mmol), 3-chlorofuro[2,3-*b*:5,4-*b'*]dipyridine (3) (1 g, 4.89 mmol), K₃PO₄ (3.11 g, 14.67 mmol), and *S*-Phos (0.3 g, 0.73 mmol) were dissolved in toluene and distilled water while bubbling with nitrogen for 30 min. Pd₂(dba)₃ (0.14 g, 0.15 mmol) was added to the solution, and the resulting solution was refluxed for 24 h under nitrogen atmosphere. The mixture was diluted with ethyl acetate and washed with distilled water. The organic layer was dried over anhydrous MgSO₄ and evaporated in vacuo to give the crude product. The extract was evaporated to dryness, affording a white solid, which was further purified by column chromatography by ethyl acetate/*n*-hexane.

Yield = 62%. *T_g* = 74 °C. *T_m* = 242 °C. ¹H NMR (500 MHz, CDCl₃): δ 8.68 (s, 1H, *J* = 2.5 Hz), 8.51 (d, 1H, *J* = 3.25 Hz), 8.38 (s, 1H, *J* = 2.5 Hz), 8.29 (d, 1H, *J* = 4.50 Hz), 7.49 (d, 2H, *J* = 4.25 Hz), 7.39 (t, 1H, *J* = 4.17 Hz), 7.29 (t, 4H, *J* = 5.33 Hz), 7.19 (d, 2H, *J* = 4.25 Hz), 7.15 (d, 4H, *J* = 4 Hz), 7.06 (t, 2H, *J* = 5 Hz). ¹³C NMR (500 MHz, CDCl₃): δ 162.1, 160.8, 148, 147.6, 147.4, 146.1, 133.5, 131, 130.4, 129.4, 128.2, 128, 124.7, 123.6, 123.3, 119.8, 115.7, 115.4. MS (FAB) *m/z*: 414 [(M + H)⁺]. Anal. Calcd for C₂₈H₁₉N₃O: C, 81.34; H, 4.63; N, 10.16; O, 3.87. Found: C, 81.35; H, 4.69; N, 10.10; O, 3.86.

Device Fabrication and Measurements. The device structure of the TADF OLEDs was indium tin oxide (ITO, 50 nm)/poly(3,4-ethylenedioxythiophene):poly(styrenesulfonate) (PEDOT:PSS, 60 nm)/4,4'-cyclohexyldienebis[*N,N*-bis(4-methylphenyl)aniline] (TAPC, 20 nm)/1,3-bis(*N*-carbazolyl)benzene (mCP, 10 nm)/3TPAPFP or 4TPAPFP:4CzIPN (25 nm)/diphenylphosphine oxide-4-(triphenylsilyl)phenyl (TSPO1, 35 nm)/LiF (1 nm)/Al (200 nm). Hole-only device structure was ITO (50 nm)/PEDOT:PSS (10 nm)/3TPAPFP or 4TPAPFP (100 nm)/TAPC (10 nm)/Al, and electron-only device structure was ITO (50 nm)/Ca (10 nm)/3TPAPFP or 4TPAPFP (100 nm)/LiF (1 nm)/Al (100 nm). TADF OLED with CBP as a host was also fabricated as a standard device, and the device structure was ITO (50 nm)/PEDOT:PSS (10 nm)/TAPC (20 nm)/mCP (10 nm)/CBP:4CzIPN (25 nm, 5%)/TSPO1 (35 nm)/LiF (1 nm)/Al (200 nm). PL measurement of the 4CzIPN-doped 3TPAPFP and 4TPAPFP films was carried out using fluorescence spectrophotometer (HITACHI, F-7000), and transient PL measurement was performed using a pulsed Nd-YAG laser (355 nm) as the excitation light source and an intensified charge-coupled device (ICCD) as a detector. Current density–voltage characteristics of the hole-only and electron-only devices were measured using Keithley 2400 source measurement unit, and the device performances of the TADF OLEDs were characterized by Keithley 2400 source measurement unit and CS 1000 spectroradiometer. Lambertian distribution of light emission was confirmed in all quantum efficiency measurement.

RESULTS AND DISCUSSION

The 4CzIPN emitter possesses a singlet energy of 2.45 eV, triplet energy of 2.40 eV, the highest occupied molecular orbital (HOMO) of −5.80 eV, the lowest unoccupied molecular orbital (LUMO) of −3.40 eV, and ultraviolet–visible (UV–vis) absorption edge of 472 nm.¹⁹ Therefore, the host materials for the 4CzIPN emitter should have higher singlet and triplet energy, deeper HOMO level, and shallower LUMO level than 4CzIPN for energy transfer and little exciton quenching. In addition, the photoluminescence (PL) emission wavelength of the host materials should be shorter than the UV–vis absorption edge of 4CzIPN for efficient energy transfer from the host materials to the 4CzIPN dopant. Moreover, bipolar host materials may be effective to balance holes and electrons in the 4CzIPN device.

The 3TPAPFP and 4TPAPFP host materials were designed to show bipolar charge transport properties, high singlet and triplet energy, appropriate HOMO/LUMO level, and PL emission for energy transfer by combining a triphenylamine moiety with a furodipyridine moiety. The furodipyridine moiety is an electron transport unit because of high electron deficiency by the two electron deficient pyridine units and possesses a high triplet energy.¹⁸ The triphenylamine moiety is a hole transport unit because of strong electron donating character of aromatic amine and has a high triplet energy. Therefore, the combination of triphenylamine with furodipyridine may produce bipolar host materials with bipolar charge transport properties and high triplet energy. In addition, the donor–acceptor structure of the host materials may reduce the singlet energy while keeping the high triplet energy of the host materials, which may be beneficial for energy transfer to the 4CzIPN dopant.

The 3TPAPFP and 4TPAPFP host materials were synthesized by Suzuki coupling reaction between boronic ester of diphenylaniline and 3-chlorofuro[2,3-*b*:5,4-*b'*]dipyridine as shown in Scheme 1. The 3-chlorofuro[2,3-*b*:5,4-*b'*]dipyridine intermediate was prepared according to the synthetic procedure reported in other work.¹⁹ Synthetic yields of 3TPAPFP and 4TPAPFP were 74% and 62%, respectively, after vacuum train sublimation. The chemical structure of the host materials was confirmed by chemical analysis, and highly pure compound with a purity of 99.9% was used for characterization and device fabrication.

Molecular simulation of 3TPAPFP and 4TPAPFP was carried out to study the HOMO and LUMO distribution of the host materials. Figure 1 shows the HOMO and LUMO distribution of 3TPAPFP and 4TPAPFP calculated by Gaussian 09 program using density functional theory of B3LYP with 6-

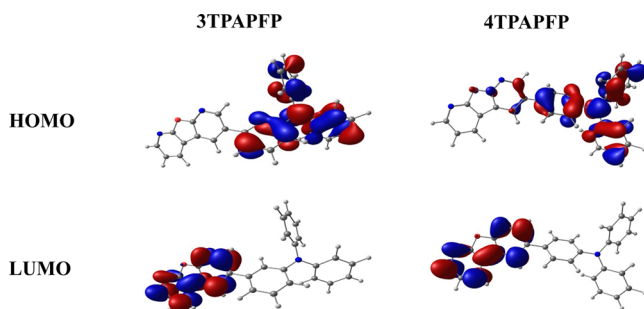


Figure 1. HOMO and LUMO distribution of 3TPAPFP and 4TPAPFP.

31G* basis sets. The HOMO of 3TPAPFP and 4TPAPFP was localized on the triphenylamine moiety, whereas the LUMO was dispersed over the PFP moiety. The HOMO and LUMO were isolated in the molecular structure because of donor–acceptor structure of 3TPAPFP and 4TPAPFP. This indicates that the 3TPAPFP and 4TPAPFP host materials may show bipolar charge transport properties and small singlet and triplet energy difference. In addition to the small singlet and triplet energy difference, narrow bandgap is also induced by the donor–acceptor character of the hosts, which is advantageous to reduce the driving voltage of the device and to optimize the device performances at low doping concentration by managing the light emission mechanism.

Figure 2 shows UV–vis absorption, solid PL, solid PL in polystyrene (PS) and low temperature PL emission spectra of

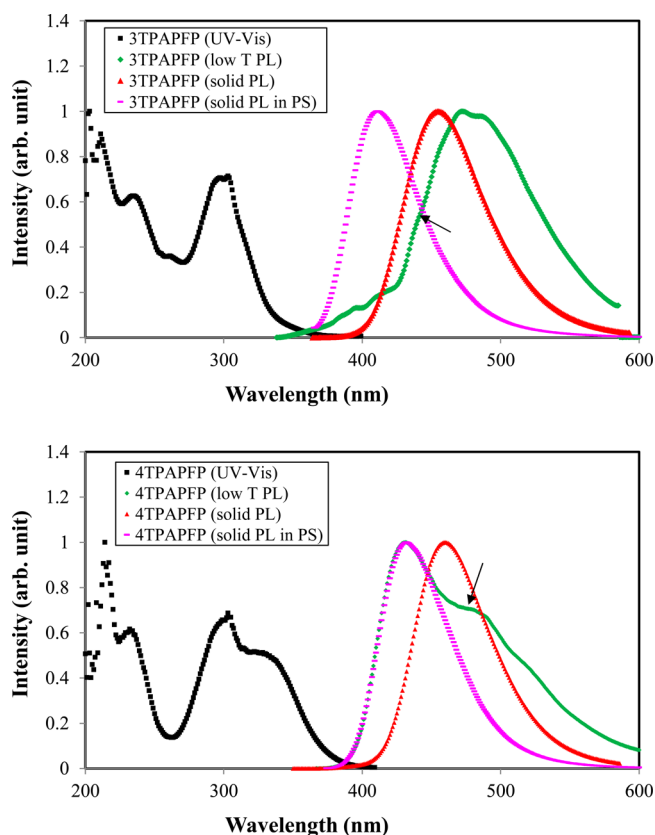


Figure 2. UV–vis, solid PL, solid PL in PS (3% doping), and low temperature PL spectra of 3TPAPFP and 4TPAPFP. Low temperature PL measurement was carried out in tetrahydrofuran solvent.

3TPAPFP and 4TPAPFP. UV–vis absorption of 4TPAPFP was observed at long wavelength compared to that of 3TPAPFP due to strong $n-\pi^*$ and $\pi-\pi^*$ absorption of the triphenylamine unit linked to furodipyridine through the para position. Singlet and triplet energies of the 3TPAPFP and 4TPAPFP host materials were calculated from the maximum emission peak of solid PL in PS and low temperature PL. Both singlet and triplet energies of 4TPAPFP were lowered compared to those of 3TPAPFP because of a large extension of conjugation through para linkage compared with the meta linkage of 3TPAPFP. Singlet/triplet energies of 3TPAPFP and 4TPAPFP were 3.02/2.82 eV and 2.88/2.63 eV, respectively. The singlet–triplet energy differences of 3TPAPFP and 4TPAPFP were only 0.20 and 0.25 eV, which were much lower than those of other

host materials and would be helpful to lower the driving voltage. The singlet energies of 3TPAPFP and 4TPAPFP were reduced in the pure solid film because of the strong intermolecular interaction, as can be seen in the bathochromic shift of the solid PL emission. The solid PL emission of 3TPAPFP and 4TPAPFP was well overlapped with the UV–vis absorption of 4CzIPN, which is extended to 472 nm, which indicates that 3TPAPFP and 4TPAPFP can transfer energy to the 4CzIPN dopant.

The HOMO/LUMO levels of 3TPAPFP and 4TPAPFP were measured by CV from oxidation and reduction curves. The HOMO/LUMO levels of 3TPAPFP and 4TPAPFP were $-5.90/-3.02$ eV and $-5.88/-2.98$ eV, respectively. The transport bandgaps from the HOMO/LUMO levels were 2.88 and 2.90 eV for 3TPAPFP and 4TPAPFP. The strong donor–acceptor character reduced the bandgap of the host materials, which is beneficial to lower the driving voltage of the devices.

Solid PL of the 4CzIPN-doped 3TPAPFP and 4TPAPFP films was measured to study the energy transfer from the 3TPAPFP host to 4CzIPN dopant. Figure 3 shows PL spectra

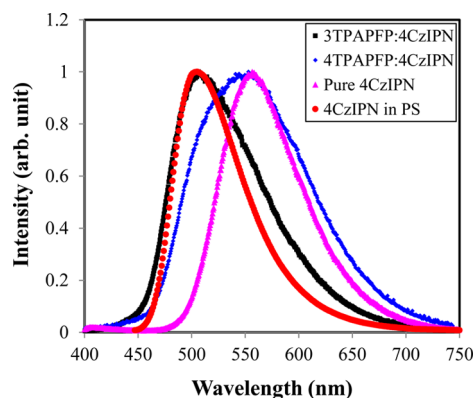


Figure 3. PL spectra of 3TPAPFP:4CzIPN, 4TPAPFP:4CzIPN, and 4CzIPN in PS and pure 4CzIPN films.

of 4CzIPN-doped 3TPAPFP and 4TPAPFP films. Doping concentration of 4CzIPN was 3 wt %. PL emission spectra of 4CzIPN-doped in PS and pure 4CzIPN film were also added to compare the PL emission of the 4CzIPN-doped 3TPAPFP and 4TPAPFP films with that of 4CzIPN. The 3TPAPFP:4CzIPN film showed typical emission of 4CzIPN at 506 nm, whereas the 4TPAPFP:4CzIPN film showed broad featureless emission with a peak maximum at 543 nm. This result indicates that the energy transfer from the 3TPAPFP host to the 4CzIPN dopant is efficient, whereas the energy transfer from the 4TPAPFP host to the 4CzIPN dopant is poor. The energy transfer efficiency of 3TPAPFP:4CzIPN was 92.0% and PL quantum efficiency was $83 \pm 4\%$. The emission of the 4TPAPFP:4CzIPN film was shifted to the PL emission wavelength of the solid PL emission of the pure 4CzIPN film. Considering the fact that the PL emission wavelengths of 4CzIPN-doped PS film and pure 4CzIPN film are around 507 and 555 nm, the broad emission of the 4TPAPFP:4CzIPN film is due partly to 4CzIPN emission and partly to exciplex formation between 4TPAPFP and 4CzIPN by strong intermolecular interaction, which is induced by strong donor–acceptor character of 4TPAPFP as can be confirmed by solvatochromic effect of the host materials (Supporting Information Figure S1). Considering the fact that the solvatochromic effect is similar in the two host materials,

the different exciplex formation is originated by geometrical effect of the molecular structure. It was reported that the para configuration induces more intermolecular interaction than meta configuration because of geometrical effects.^{20,21} Therefore, the exciplex formation between host and highly polar 4CzIPN was significant in the 4TPAPFP:4CzIPN film. The exciplex formation was relatively weak in the 3TPAPFP:4CzIPN film.

To confirm singlet emission by reverse intersystem crossing from triplet state to singlet state, delayed fluorescence of the 3TPAPFP:4CzIPN film was measured. Delayed PL spectra of the 3TPAPFP:4CzIPN film are shown in Figure 4. Delay time

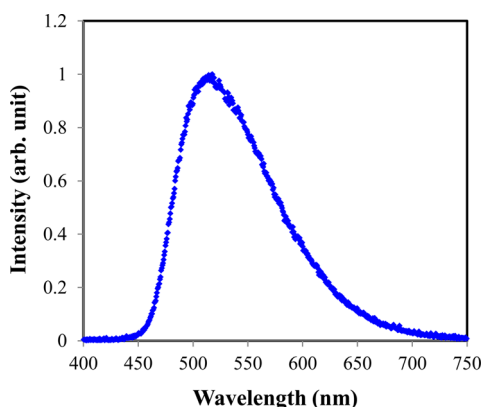


Figure 4. Delayed PL spectrum of 3TPAPFP:4CzIPN film (delay time 1 μ s).

was 1 μ s. The 3TPAPFP:4CzIPN film showed delayed PL emission at the same wavelength of the room temperature PL emission of 3TPAPFP:4CzIPN film, implying reverse intersystem crossing from triplet state to singlet state as reported in Adachi's work.⁵ The 3TPAPFP host activated the TADF emission of 4CzIPN through efficient energy transfer and little triplet exciton quenching. The high singlet and triplet energies of the 3TPAPFP host suppressed exciton quenching of 4CzIPN.

Transient PL measurement of the 4CzIPN-doped 3TPAPFP film was carried out to investigate the light emission process of the 3TPAPFP:4CzIPN film. Figure 5 shows transient PL curve of the 3TPAPFP:4CzIPN film. Excited state lifetime of the delayed fluorescence was calculated from the transient decay curve of the film, and it was 5.0 μ s. The lifetime of the

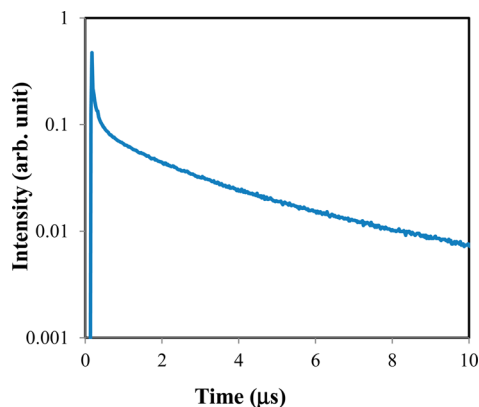


Figure 5. Transient PL spectrum of 3TPAPFP:4CzIPN film.

3TPAPFP:4CzIPN film was similar to that of 4CzIPN, indicating efficient energy transfer and TADF emission of the 4CzIPN dopant.⁵

Based on the basic photophysical properties of 3TPAPFP and 4TPAPFP, they were evaluated as the host materials for the 4CzIPN dopant. The device structure was indium tin oxide (ITO, 50 nm)/poly(3,4 ethylenedioxythiophene):poly(styrenesulfonate) (PEDOT:PSS, 60 nm)/4,4'-cyclohexylidenebis[*N,N*-bis(4-methylphenyl)aniline] (TAPC, 20 nm)/1,3-bis(*N*-carbazolyl)benzene (mCP, 10 nm)/3TPAPFP or 4TPAPFP:4CzIPN (25 nm)/diphenylphosphine oxide-4-(triphenylsilyl)phenyl (TSPO1, 35 nm)/LiF (1 nm)/Al (200 nm). The doping concentrations of 4CzIPN were 1% and 2% in the 3TPAPFP and 4TPAPFP devices, respectively, after optimizing the doping concentration. Figure 6 shows

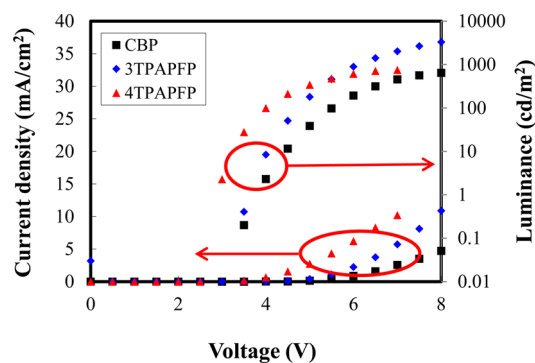


Figure 6. Current density–voltage–luminance curves of 3TPAPFP, 4TPAPFP, and CBP devices.

current density–voltage–luminance curves of 3TPAPFP and 4TPAPFP devices doped with 4CzIPN in comparison with that of the CBP device. As the device performances of the 3TPAPFP and 4TPAPFP devices were optimized at 1% and 2% doping concentrations, respectively, the device performances at optimum doping concentration were compared. Device data at other doping concentrations of 3TPAPFP devices are appended in Figure S2 in Supporting Information. Optimum doping concentration of the CBP device was 5%. The 4TPAPFP device showed higher current density than the 3TPAPFP device because of high electron current density of the 4TPAPFP device as shown in single carrier device data of 3TPAPFP and 4TPAPFP (Figure 7) and intermolecular charge transfer complex formation between 4TPAPFP and 4CzIPN. Although the current density of the 3TPAPFP device was lower

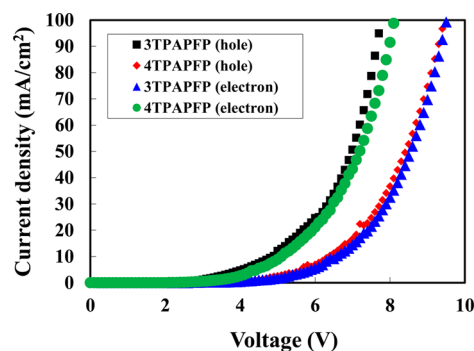


Figure 7. Current density–voltage curves of hole-only and electron-only devices of 3TPAPFP and 4TPAPFP.

than that of the 4TPAPFP device, both devices showed higher current density than the CBP device because of bipolar charge transport properties of the host materials, low energy barrier for charge injection due to shallow HOMO and deep LUMO levels, and intermolecular charge transfer complex formation originated by donor–acceptor character of the materials. The luminance was also high in the 4TPAPFP device because of high current density.

Quantum efficiency–current density curves of 3TPAPFP and 4TPAPFP devices are shown in Figure 8. The quantum

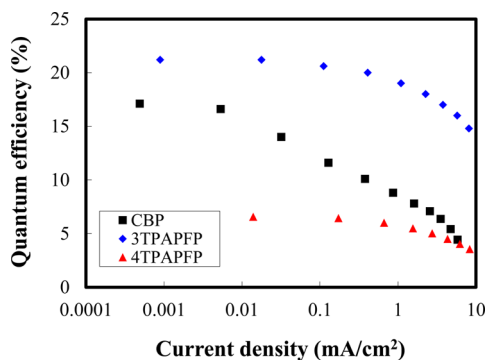


Figure 8. Quantum efficiency–luminance curves of 3TPAPFP, 4TPAPFP, and CBP devices.

efficiency of the 3TPAPFP device was higher than that of the 4TPAPFP device, and the maximum quantum efficiency of the 3TPAPFP device was 21.2%. The quantum efficiency of the 3TPAPFP device was higher than that of the CBP device with the same 4CzIPN dopant. In particular, the quantum efficiency of the 3TPAPFP device was much higher than that of the CBP device at high luminance. The high quantum efficiency of the 3TPAPFP device can be explained by the bipolar charge transport properties, efficient energy transfer from the 3TPAPFP host to the 4CzIPN dopant, activation of delayed fluorescence, and charge and exciton confinement in the emitting layer. As shown in the single carrier device data, the 3TPAPFP host showed bipolar charge transport properties because of hole transport type triphenylamine and electron transport type PFP units. The bipolar charge transport properties of 3TPAPFP host balanced holes and electrons in the emitting layer and improved the quantum efficiency of the 3TPAPFP device. Efficient energy transfer from the 3TPAPFP host to the 4CzIPN dopant also improved the quantum efficiency of the 3TPAPFP device. Singlet and triplet energy transfer from the 3TPAPFP to 4CzIPN was efficient as confirmed by PL measurement. In addition, the 3TPAPFP host activated the TADF emission of 4CzIPN as presented in transient PL spectrum, resulting in high quantum efficiency above 20%. Other than these, blocking of charge leakage due to high energy barrier for charge leakage induced by narrow bandgap of the host materials, suppression of singlet and triplet exciton quenching by host, and charge transport material were also important factors for the high quantum efficiency. Device performances are summarized in Table 1.

The efficient energy transfer optimized the quantum efficiency of the 3TPAPFP device at a very low doping concentration of 1% compared with 5% of CBP device in other work⁵ and in our experiment. The low optimum doping concentration can be explained by the device structure with little energy barrier for charge injection. Energy transfer

Table 1. Device Performances of CBP, 3TPAPFP, and 4TPAPFP Devices^a

| | driving voltage (V) ^b | maximum quantum efficiency (%) | quantum efficiency (%) ^b | color coordinate ^b |
|---------|----------------------------------|--------------------------------|-------------------------------------|-------------------------------|
| CBP | 7.2 ± 0.1 | 17.1 ± 0.3 | 6.8 ± 0.2 | (0.21,0.53) |
| 3TPAPFP | 5.5 ± 0.1 | 21.2 ± 0.4 | 18.8 ± 0.3 | (0.19,0.43) |
| 4TPAPFP | 5.6 ± 0.1 | 6.6 ± 0.2 | 4.4 ± 0.3 | (0.34,0.50) |

^aThree samples were used for the statistical measurement of the data.

^bData was measured at 500 cd/m².

dominates the light emission of the 3TPAPFP device because there is no energy barrier for hole injection from mCP to 3TPAPFP or for electron injection from TSPO1 to 3TPAPFP as shown in energy level diagram in Figure 9. Therefore, the

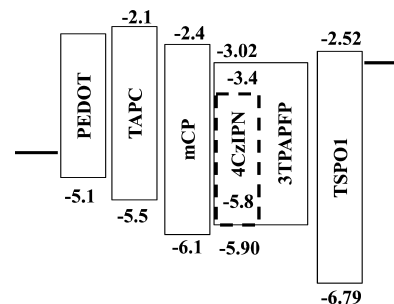


Figure 9. Energy level diagram of 3TPAPFP:4CzIPN devices.

device performances are optimized at a doping concentration of 1%, which minimizes exciton quenching. As reported in other works,²² the device performances cannot be optimized at low doping concentration if charge trapping dominates the light emission process. The strong donor–acceptor character, which induces small singlet–triplet energy gap and narrow bandgap, enabled the development of the TADF device with very low optimum doping concentration of 1%. The optimum doping concentration of the 4CzIPN device was similar to that of common green fluorescent OLEDs.

In addition to the high quantum efficiency and low optimum doping concentration, efficiency roll-off was significantly improved in the 3TPAPFP device compared with CBP device. The quantum efficiency at 500 cd/m² of the 3TPAPFP device was 18.8% compared with the maximum quantum efficiency of 21.2%, and the efficiency reduction from the maximum quantum efficiency was only 11%. However, the quantum efficiency of the CBP device was sharply dropped, and the quantum efficiency at 500 cd/m² was only 6.8% compared with maximum quantum efficiency of 17.1%. The bipolar charge transport properties of the 3TPAPFP host improved the efficiency roll-off of the 3TPAPFP device. The poor quantum efficiency of the 4TPAPFP device is due to strong exciplex formation between 4TPAPFP host and 4CzIPN, as shown in the PL spectra of the 4CzIPN-doped 4TPAPFP film.

Electroluminescence (EL) spectra of CBP, 3TPAPFP, and 4TPAPFP devices doped with 4CzIPN are shown in Figure 10. EL emission peak of 3TPAPFP:4CzIPN was shifted to a short wavelength compared to that of the CBP:4CzIPN device because of the low optimum doping concentration of 1%, whereas the emission peak of the 4TPAPFP:4CzIPN device was shifted to a long wavelength due to exciplex emission from the device. No host emission from 3TPAPFP was observed in the EL spectra, which proves efficient energy transfer of the

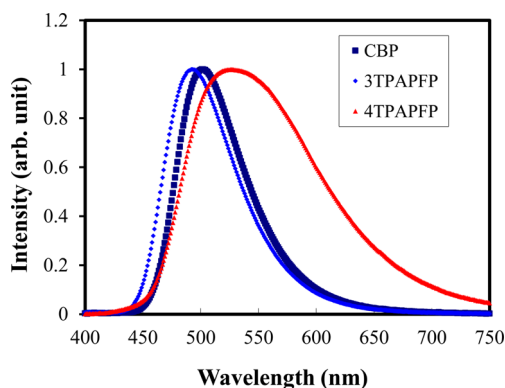


Figure 10. Electroluminescence spectra of 3TPAPFP:4CzIPN, 4TPAPFP:4CzIPN, and CBP:4CzIPN devices.

3TPAPFP:4CzIPN device. The color coordinates of the CBP:4CzIPN, 3TPAPFP:4CzIPN, and 4TPAPFP:4CzIPN devices were (0.21, 0.52), (0.19, 0.43), and (0.36, 0.52), respectively.

CONCLUSIONS

In conclusion, highly efficient green TADF OLEDs with a quantum efficiency above 20% were developed using 3TPAPFP host material with a singlet and triplet energy for efficient energy transfer and bipolar charge transport properties for balanced hole and electron density. The 3TPAPFP device doped with the 4CzIPN dopant showed a high quantum efficiency of 21.2%, a low optimum doping concentration of 1%, and a small efficiency roll-off of 16%. Therefore, it was proven that TADF OLEDs would show comparable device performances to phosphorescent OLEDs. It is expected that the quantum efficiency of the 4CzIPN device can be improved by developing better host materials for the TADF dopant.

ASSOCIATED CONTENT

Supporting Information

PL spectra and current density–voltage–luminescence plots. This information is available free of charge via the Internet at <http://pubs.acs.org/>.

AUTHOR INFORMATION

Corresponding Author

*J. Y. Lee. E-mail: leej17@dankook.ac.kr. Tel.: 82-31-8005-3585. Fax: 82-31-8005-3585.

Notes

The authors declare no competing financial interest.

REFERENCES

- (1) Baldo, M. A.; O'Brien, D. F.; You, Y.; Shoustikov, A.; Sibley, S.; Thompson, M. E.; Forrest, S. R. *Nature* **1998**, *395*, 151.
- (2) Zhen, C.; Dai, Y.; Zeng, W.; Ma, Z.; Chen, Z.; Kieffer, J. *Adv. Funct. Mater.* **2011**, *21*, 699.
- (3) Wei, Y.; Chen, C. T. *J. Am. Chem. Soc.* **2007**, *129*, 7478.
- (4) Okumoto, K.; Kanno, H.; Hamaa, Y.; Takahashi, H.; Shibata, K. *Appl. Phys. Lett.* **2006**, *89*, 063504.
- (5) Uoyama, H.; Goushi, K.; Shizu, K.; Nomura, H.; Adachi, C. *Nature* **2012**, *492*, 234.
- (6) Kondakov, D. Y.; Pawlik, T. D.; Hatwar, T. K.; Spindler, J. P. *J. Appl. Phys.* **2009**, *106*, 124510.
- (7) King, S. M.; Cass, M.; Pintani, M.; Coward, C.; Dias, F. B.; Monkman, A. P.; Roberts, M. *J. Appl. Phys.* **2011**, *109*, 074502.

(8) Dias, F. B.; Bourdakos, K. N.; Jankus, V.; Moss, K. C.; Karntekar, K. T.; Bhalla, V.; Santos, J.; Bryce, M. R.; Monkman, A. P. *Adv. Mater.* **2013**, *25*, 3707.

(9) Goushi, K.; Yoshida, K.; Sato, K.; Adachi, C. *Nat. Photonics* **2012**, *6*, 253.

(10) Zhang, Q.; Li, J.; Shizu, K.; Huang, S.; Hirata, S.; Miyazaki, H.; Adachi, C. *J. Am. Chem. Soc.* **2012**, *134*, 14706.

(11) Li, J.; Nakagawa, T.; Zhang, Q.; Nomura, H.; Miyazaki, H.; Adachi, C. *Adv. Mater.* **2013**, DOI: 10.1002/adma.201300575.

(12) Lee, S. Y.; Yasuda, T.; Nomura, H.; Adachi, C. *Appl. Phys. Lett.* **2012**, *101*, 093306.

(13) Nakagawa, T.; Ku, S.-Y.; Wong, K.-T.; Adachi, C. *Chem. Commun.* **2012**, *48*, 9580.

(14) Méhes, G.; Nomura, H.; Zhang, Q.; Nakagawa, T.; Adachi, C. *Angew. Chem., Int. Ed.* **2012**, *51*, 11311.

(15) Tanaka, H.; Shizu, K.; Miyazaki, H.; Adachi, C. *Chem. Commun.* **2012**, *48*, 11392.

(16) Czerwieńiec, R.; Yu, J.; Yersin, H. *Inorg. Chem.* **2011**, *50*, 8293.

(17) Yersin, H.; Rausch, A. F.; Czerwieńiec, R.; Hofbeck, T.; Fischer, T. *Coord. Chem. Rev.* **2011**, *255*, 2622.

(18) Lee, C. W.; Lee, J. Y. *Chem. Commun.* **2013**, *49*, 6185.

(19) Nakanotani, H.; Masui, K.; Nishide, J.; Shibata, T.; Adachi, C. *Sci. Rep.* **2013**, *3*, 2127.

(20) Huang, J.; Sun, N.; Dong, Y.; Tang, R.; Lu, P.; Cai, P.; Li, Q.; Ma, D.; Qin, J.; Li, Z. *Adv. Funct. Mater.* **2013**, *23*, 2329.

(21) Zhu, M.; Yang, C. *Chem. Soc. Rev.* **2013**, *42*, 4963.

(22) Seo, C. W.; Yoon, J. H.; Lee, J. Y. *Org. Electron.* **2012**, *13*, 341.